Electrodeless Helicon Plasma Thruster Employing Additional Electromagnetic Acceleration Methods

IEPC-2019-A-198

Presented at the 36th International Electric Propulsion Conference
University of Vienna • Vienna, Austria
September 15-20, 2019

T. Furukawa[1], K. Shimura, K. Hachisu, S. Shinohara
Tokyo University of Agriculture and Technology, Koganei, Tokyo, 184-8588, Japan

S. Yamamura[2]
The University of Tokyo, Kashiwa, Chiba, 277-0882, Japan

and

D. Kuwahara[3]
Chubu University, Kasugai, Aichi, 487-8501, Japan

Abstract: We are proposing an electrodeless additional plasma acceleration scheme, i.e., Rotating Magnetic Field (RMF) and *m* = 0 half-cycle additional plasma accelerations. In these acceleration schemes, additional plasma acceleration mechanism is adopted to enhance evacuation of a plasma flow in typical rf/helicon plasma thrusters. Here, the thrust performance can be improved, compared to conventional rf/helicon plasma thrusters, in which thermal thrust (magnetic nozzle effect) governs the total thrust generation mechanism. In our electrodeless condition, no electrodes directly contact with a plasma, leading to no erosion of the electrodes expected in generating/accelerating plasmas. In our proposed additional acceleration schemes, an electromagnetic force can be generated with the RMF application into the plasma, which is eventually evacuated outside of the thruster system, leading to a thrust. In the RMF scheme, we demonstrated an azimuthal current drive, which is necessary to generate the electromagnetic force inside of the plasma, by measuring spatiotemporal profiles of the time-varying RMF. We are also proposing *m* = 0 half-cycle acceleration system. Here, we use a loop antenna having several turns, to induce an azimuthal current due to the correlation between applied coil magnetic field and generated plasma. Experimental results of both acceleration schemes will be presented in this conference.

Nomenclature

m	=	azimuthal mode number
v_i	=	ion velocity
n_e	=	electron density
j_θ	=	azimuthal current density
I_{m0}	=	m = 0 coil current
fr	=	gas flow rate
ϕ	=	current phase difference between two sets of RMF antennas
f_{m0}	=	alternated current (ac) frequency applied to a m = 0 coil
T_{m0}	=	m = 0 ac current period
P_{rf}	=	rf (radio frequency) power
I_{RMF}	=	ac current applied to RMF coils
f_{RMF}	=	ac RMF current frequency

$j_{diamag.}$ = diamagnetic current density

I.Introduction

Recent space missions have been showing remarkable improvement of space propulsion technique. Especially, all-electronic satellites and cube-sats, which are a kind of miniatured space modules, are widely launched all over the world, using electric thrusters. As a famous future trial, manned expedition to the Mars is seriously considered so as to develop and create the second habitual planet. However, such a manned space mission is not so easy to be carried out at the present stage, because thrust performance of current space propulsion system is not so sufficient that people cannot spend their limited times inside the space module, in terms of the power limitation and the relatively long-term mission.

Electrodeless plasma propulsion concept is a candidate of next-generation space propulsion systems. Conventional electric thruster schemes, e.g., ion gridded thruster[1] and Hall thruster,[2] have erosion of electrodes (grids), leading to degradation of the thrust performance and the limitation of thruster lifetime. These problems make future space developments, e.g., further away space probe, construction of solar energy device, and transportation of human beings to the next habitual planet, etc., difficult, and delay of space science achievement. Despite such a disadvantage in the conventional electric thrusters, many space missions have been being fulfilled by the use of the present propulsion technique. Nevertheless, for the future space development, we have to create other space propulsion schemes considering the lifetime limitation and the performance. Needless to say, high-power system with stable and reliable conditions must be pursued

As a representative electrodeless plasma prolusion system, VAriable Specific Impulse Magnetoplasma Rocket (VASIMR)[3,4] is being researched and developed. In this scheme, high-dense plasma can be generated by a helicon wave propagation,[5] and the generated plasma is supposed to be accelerated in the presence of the divergent external magnetic field (so-called, magnetic nozzle shape) after being energized by Ion Cyclotron Resonance Heating (ICRH) section. Up to 72 % and 6 N of the thrust efficiency and the thrust values were, respectively, obtained despite high-power use of 200 kW-class power supply so far.[3]

Novel electrodeless plasma propulsion methods, in which an additional plasma acceleration scheme is adopted in a typical rf/helicon[5] plasma thruster scheme, have been proposed under Helicon Electrodeless Advanced Thruster (HEAT) project proposed by *Shinohara et al*.(see e.g., Refs. 6,7) One of the main purposes of this project is to enhance the thrust performance in the typical rf/helicon-base high-dense plasma thruster. Basically, its main acceleration mechanism in this simple thruster is thermal acceleration owing to a magnetic nozzle.[8,9] According to several experimental approaches in electrodeless thruster concept by *Takahashi et al*,[9] the thermal thrust term has an upper threshold indicating the limitation of the performance with only using the nozzle effect. Among them, Rotating Magnetic Field (RMF)[10,11] and $m = 0$ half-cycle plasma acceleration methods[12,13] have been being studied at Tokyo University of Agriculture and Technology as candidates expected to enhance the thrust performance, as additional acceleration schemes applied, using the simple thruster. Our present purpose is the proof of the principles of these two concepts, and here, experimental results will be shown in this conference.

In our RMF experimental scheme, time-varying, rotating B-field is applied perpendicular to a plasma column outside of a discharge tube (mainly, we use a quartz tube). How to generate the RMF will be shown in next section. Note that plasma itself is generated by the use of an external rf antenna and external steady B-field with the plasma density of from 10^{10} to 10^{12} cm^{-3}. In our scheme, helicon mode can be obtained by using an axially uniform B-field configuration and higher rf power. Electrons are expected to be accelerated azimuthally in the presence of a dc azimuthal electric field induced by non-linear effect, so-called, the Hall term effect, leading to an electron azimuthal current in the plasma column. Hereby, the plasma can be electromagnetically accelerated by the axial Lorentz force caused by a cross product of the driven current and a radial component of an external divergent B-field. In our previous experimental trial, increments of ion velocity, v_i and also, electron density, n_e were found with RMF application, up to 32 and 160 %, respectively.[14] This result suggested that the RMF method could contribute to plasma thrust even though the performance should be more enhanced. Despite such a low performance, the azimuthal current drive has also been demonstrated through spatiotemporal measurements of the time-varying B-field for several experimental conditions, and the additional electromagnetic force in the RMF antenna region was confirmed for the first time.[15] We suggested that higher RMF strength and lower ac RMF applied current frequency are expected to contribute to the plasma acceleration effect from the view point of the RMF penetration condition into plasma.[16]

We are also proposing $m = 0$ half-cycle plasma acceleration method, which is also a kind of the electromagnetic plasma accelerations.[7,12,13] Here, m means an azimuthal mode number. Its acceleration mechanism is different from the RMF ones: We have applied this acceleration scheme to the Small Helicon Device (SHD).[17] Diameter of a quartz tube is from 1 to ~30 mm.[11] This small size scale was considered to be applied to small size plasma thruster scheme, e.g., cube-sat and miniature thruster concept. As same as the RMF concept, an azimuthal current can be induced by using a $m = 0$ coil, which has several turns and externally generate time-varying magnetic field outside of the discharge tube. Then, the axial Lorentz force can be generated leading to the electromagnetic plasma acceleration. Here, we will present the conceptual experimental results, including spatiotemporal plasma generation and acceleration mechanisms in the vicinity of the acceleration antenna region, in addition to the dependences of the plasma parameters on an external plasma B-field strength. We have found density-peaked profiles near the generation antenna in the presence of high external B-filed strength (< 600 A_{pp}) induced by the $m = 0$ coils. This tendency is expected to be caused by the magnetic pressure, which push the generated plasma flow to the downstream region, as well as the original force effect. The spatial acceleration effect can be optimized by choosing suitable operational conditions. In both two cases of RMF and $m = 0$ acceleration schemes, the azimuthal current is essential to obtain the additional acceleration effect. Note that these two concepts are totally different from Magneto-Plasma Dynamic (MPD) thruster from the view point of the existence of electrodes.

Our current interest is to clarify the plasma acceleration mechanism and the acceleration effect with both electrodeless acceleration concepts. Present experimental approaches are based on the physical processes including how the plasma can be accelerated and generated, in the proposed plasma acceleration schemes. Note that the thrust performances of the additional plasma acceleration concepts are not enough to be utilized in space at the present stage but those have a possibility to change the conventional concept of the space propulsion largely, and the present experiment can be a milestone for the next experimental approach.

The outline of the rest of this paper is the followings: Explanation of the proposed additional plasma acceleration methods and the schemes are described in Secs. II and III, respectively. Section IV shows experimental results regarding the two acceleration concepts, followed by Conclusion in Sec. V.

II. Additional Plasma Acceleration methods

A. RMF acceleration method

In our experimental conditions, two sets of opposed facing coils are used to induce the RMF, as shown in Fig. 1. Inside a cylindrical plasma, here, ions are assumed to be immovable and electron inertia can be neglected. In the presence of the plasma, an axial screening oscillating current is induced due to the plasma resistivity. Under the generalized Ohm's law, the Hall term has ac and dc components, and azimuthal electric field is induced. Hereby, only electrons are expected to start rotating azimuthally by applying the RMF, whose frequency value is between ion and electron cyclotron frequencies. Then, an azimuthal dc electron current density, j_θ, can be driven. For the additional plasma acceleration, external divergent magnetic field is applied to generate the axial Lorentz force derived from a cross product of j_θ and a radial component of the external B-field. Detailed explanation of the acceleration mechanism is described in Refs. 14–16. To obtain the ideal RMF plasma acceleration effect, penetration condition of the RMF into a plasma is also important. According to Milroy's expression,[10] RMF operational condition such as RMF applied current, I_{RMF}, the current frequency, f_{RMF}, a target plasma density, and a temperature, should be optimized, and high I_{RMF} and low f_{RMF} and low plasma density are favorable. After achievement of the full penetration condition, however, high-dense plasma is necessary to enhance the total thrust force, and therefore, we have to consider a tradeoff of these experimental conditions. Here, dependence of plasma acceleration on I_{RMF} increase, which is one of the important parameters to enhance the RMF acceleration effect, has also been investigated.

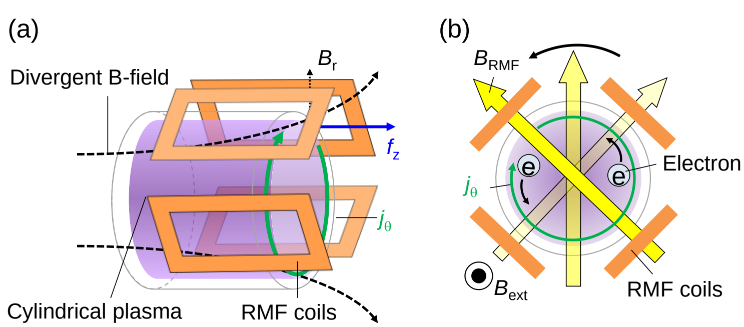

Figure 1. Schematic of (a) Lorentz force generation by the RMF method and (b) cross sectional view.

B. *m* = 0 half-cycle acceleration method

In the *m* = 0 acceleration scheme, an azimuthal current can be induced in a plasma by using a loop-type coil wound around a quartz tube, as shown in Fig. 2. This acceleration scheme is easy to develop, that makes possible to apply to such miniature thruster designs. We apply ac current, I_{m0}, (hundreds of A_{pp}) with relatively low frequency from several hundreds of Hz to several kHz, to the coil, employing the electromagnetic plasma acceleration. In this scheme, plasma can be accelerated forward to the thruster exit during a half-period of the applied oscillating current, considering the direction of radial component of the external B-field. On the contrary, during the latter half of the period, an effective backward axial force is not expected to be generated. This is because the decelerated plasma flow hits the inner discharge wall, causing no net force.

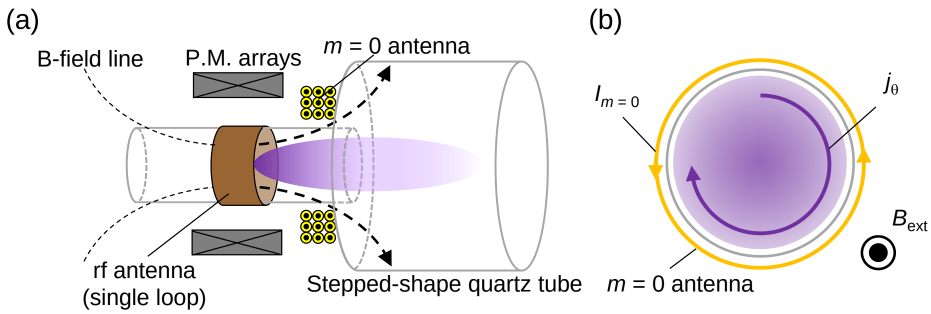

Figure 2. *m* = 0 plasma acceleration scheme [(a) acceleration concept and (b) cross sectional view].

III.Experimental devices and setup

Almost all experimental campaigns have been conducted by using rf plasma generation devices, i.e., Large Mirror Device (LMD)[18] and Small Helicon Device (SHD) at Tokyo University of Agriculture and Technology. External magnetic field shape and strength can be changed by using permanent magnets arrays and electromagnetic coils. Helicon plasma, in which high density more than 10^{13} cm^{-3}, can be easily obtained, using high radio frequency (rf) power and gas flow rate (*fr*). Such a high plasma density is important to achieve a high plasma thrust density although in this case, this acceleration effect mainly depends on the thermal thrust derived from the plasma density and temperature increments. As a plasma generation antenna, we typically use a half-helical type or a single loop-type antennas wound around a quartz tube. Here, these two additional plasma acceleration schemes are introduced as follows.

A. RMF acceleration scheme

Time-varying RMF can be generated by the use of two sets of opposed facing coils wound around a quartz tube equipped in the LMD, as shown in Fig. 3. As the rf plasma generation scheme, half-helical type antenna is wound around a quartz tube. Here, the rf discharge duration is 75 ms. Alternating current is applied to the two sets of coils and the rotation motion of applied magnetic field can be expected owing to the current phase difference, ϕ, between the different sets. We can change ϕ and get different rotational direction or oscillating one of the RMF, as shown in Fig. 4. Here, we apply the 25 ms RMF application 35 ms after the rf plasma generation discharge. The RMF method is expected to cause the electromagnetic plasma acceleration owing to the axial Lorentz force, as mentioned above. To create the acceleration effect, PM arrays, which consists of N35 (Neo Mag Co. Ltd.) covered by stainless metal frame, are mounted above the rf antenna with a spatial distance. The PM arrays have cusp-like magnetic field configuration around the center region of the chamber, as shown in Fig. 3. This shape creates the magnetic nozzle in a downstream region, leading to the Lorentz force if combined with the induced j_θ. As a side effect of the RMF method, plasma density increases by the RMF application, that is expected to cause additional plasma acceleration effects: Diamagnetic effect can come from the radial density gradient due to the B-field divergence, and the axial gradient along the *z*-axis of the plasma column. Generated plasma can be accelerated by these mechanisms, and evacuated from the tapered quartz tube region (see Fig. 3) to the vacuum chamber, in which two Turbo Molecular Pumps (TMPs) in addition to two rotary pumps as a rough vacuuming are installed. Typical background pressure w/o gas is several 10^{-4} Pa. A gas inlet is in the end of the tube head (upstream region), feeding Argon (Ar) gas controlled by a mass flow controller. In this experiment, 40-sccm Ar gas is fed continuously, and the background pressure is increased up to ~10^{-1} Pa.

A two-dimensional (2D) scanning instrument installed inside of the chamber.[19] Each probe can be mounted on the instrument, and enable to measure spatial profiles of plasma parameters and time-varying magnetic fields caused by the RMF antennas. Here, we evaluate these measured values and check the additional plasma acceleration effect.

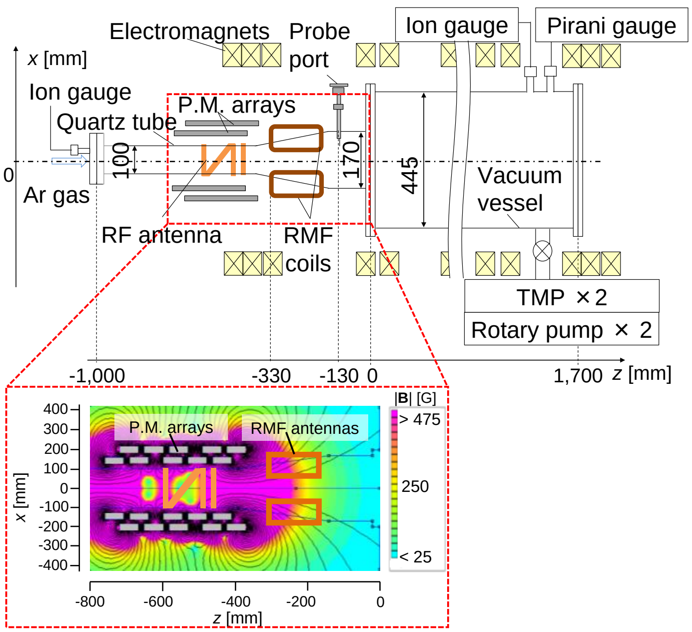

Figure 3. Schematic view of RMF acceleration scheme with an enlarged picture of PM B-field configuration and strength in the LMD.

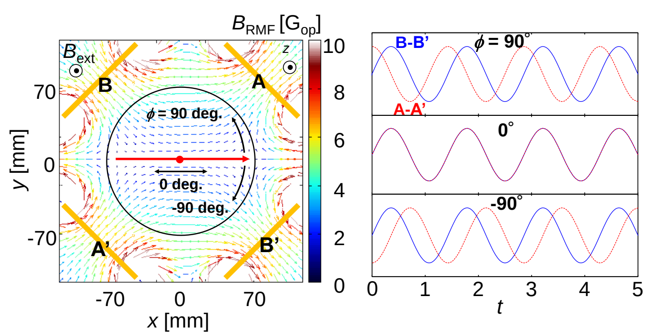

Figure 4. Dependence of the RMF rotation direction on ϕ.

B. *m* = 0 half-cycle acceleration scheme

The $m = 0$ acceleration method has been examined in the SHD, whose total axial length and chamber diameter are 1,300 mm and 165.2 mm, respectively. Plasma can be generated by using a single-loop type antenna wound around a step-shaped quartz tube, whose smaller inner diameter is 20 mm, as shown in Fig. 5. The stepped shape is expected to increase the total plasma thrust proportional to the square of thrust diameter and decrease a wall loss of the plasma as well. As an evacuation system, we use a TMP and a rotary pump connected to the side of the vacuum chamber. Typical back ground pressure of several 10^{-4} Pa can be achieved without propellant feeding. The propellant *fr* is controlled by a mass flow controller, and the maximum *fr* of 50 sccm is used. Plasma discharge is conducted by using an rf antenna wound around a 20-mm diam. quartz tube (here, we can change a diameter of the tube, easily). As an external B-field source, permanent magnet arrays are mounted, as shown in Fig. 5. Here, the B-field source is in the upstream region of the $m = 0$ coil to create a divergent DC field shape around the acceleration antenna. Argon gas is fed in the head of the quartz tube, and typical Argon pressure in the head region is ~10^{-1} Pa for the flow rate of 10 sccm. We apply an rf power, P_{rf}, up to 3 kW by the use of a Thamway high power rf source (T162-6746A), with rf frequency range is from 0.3 to 13.56 MHz, that is the same power source in the RMF acceleration scheme.

To measure plasma parameters inside of the acceleration system, we mainly use electrostatic probe methods, i.e., Mach probe and Langmuir probe methods, and the 2D spatiotemporal profiles of an electron density and an ion velocity are measured by the above probes to check the plasma acceleration effect. These signals are monitored by the use of a HIOKI Memory HiCORDER 8855 and data are stored at every plasma discharge. The alternating current applied to the m = 0 antenna is controlled by an ac amplifier instrument developed in our group,[12] and we can also change the current amplitude, I_{m0}, frequency, f_{m0}, and application period, T_{m0}, etc., by using the instrument. Note that these signal waveforms, including the voltage applied to the coil are monitored to check the phase differences and amplitudes of I_{m0}. Hereby, dependences of the plasma parameters on such operational parameters are investigated under the condition of I_{m0} up to 600 A_{pp} applied with f_{m0} of 1.5 kHz. Here, we will discuss spatial profiles of v_i and n_e measured by the use of a Mach Probe.

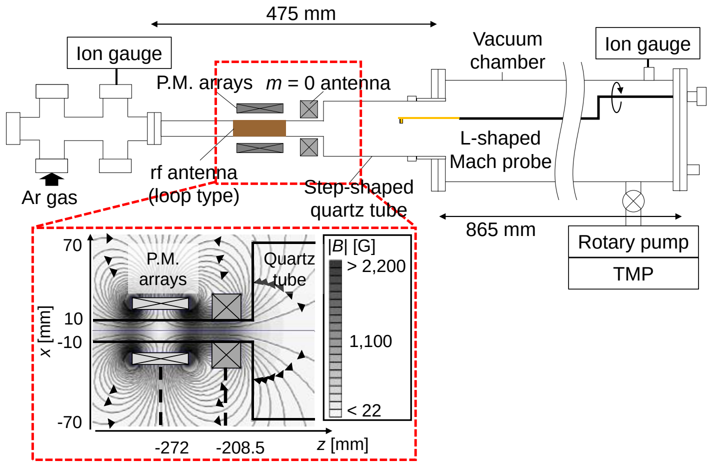

Figure 5. Schematic view of *m* = 0 acceleration scheme with an enlarged picture of PM B-field configuration and strength.

IV.Experimental results

A. Experimental results of RMF acceleration method

A-1. Spatial profiles of v_i and n_e

To investigate the acceleration effect, spatial profiles of v_i and n_e were measured by the use of a Mach probe in a downstream region of the RMF antenna. Figure 6 shows the spatial profiles for the case of P_{rf} = 1 kW, fr = 40 sccm [(a) w/o RMF], f_{RMF} = 0.7 MHz, I_{RMF} = (a) 0 (w/o RMF), (b) 55, and (c) 90 A_{pp}, and ϕ = 90°. The v_i and n_e were increased by the RMF application. Increasing rate of the v_i up to ~150 % was obtained in the downstream region of the RMF antennas for the I_{RMF} of 90 A_{pp} case. On the other hand, in the upstream acceleration region, n_e increment was evident, and its increasing rate of up to ~300 % was found. These results indicate that plasma acceleration can be also achieved by the plasma generation, i.e., a diamagnetic current effect derived from a radial density gradient of the cylindrical plasma, and an axial plasma pressure gradient which pushes the plasma plume toward the thruster exit. Figure 6 shows the radial and axial density gradients calculated from the n_e profiles for the case of w/o and w/ RMF conditions using I_{RMF} = 90 A_{pp}. The radial density gradient dominates and the magnitude is approximately 100 times larger than axial one as shown in Fig. 8. Calculated values of induced diamagnetic current density, $j_{diamag.}$, w/o and w/ the RMF are also shown in Fig. 7. The diamagnetic acceleration effect can be expected due to the profiles, and the electromagnetic force is ~6 mN derived from 2D spatial gradient in the RMF antenna region, using the product of the current density and radial component of the external PM B-field. As future works, direct thrust measurement using a target type thrust stand is required to confirm the contributions to the thrust performance as well as the RMF original electromagnetic acceleration effect.

In terms of the plasma generation efficiency with the RMF application, ratio of the density increment to a total applied power was estimated. For I_{RMF} of 55 A_{pp} case, the total RMF input power applied (difference between rf forward and reverse powers), which is a sum of these of the A and B coils shown in Fig. 4, was ~2.5 kW, and therefore, the ratio of n_e to the power of 6 [10^{10} cm^{-3}/kW] was obtained. With increasing I_{RMF} value up to 90 A_{pp}, the density increment became higher, and the ratio was 20 [10^{10} cm^{-3}/kW]. This high peaked plasma density profile in the radial direction is favorable since wall loss of the plasma can be suppressed, having the plasma evacuation efficiency to be larger with respect to the total plasma thrust. As described above, the increasing rate of v_i was also higher by increasing I_{RMF}, but the rate was much smaller than those of n_e. That can imply that plasma generation owing to the RMF application would be much evident than that the expected original RMF acceleration. However, electromagnetic force has been confirmed through spatial measurement of oscillating component of the RMF. Here, we have successfully demonstrated that the higher current generation by increasing the RMF strength with I_{RMF} increment, as shown in the next section.

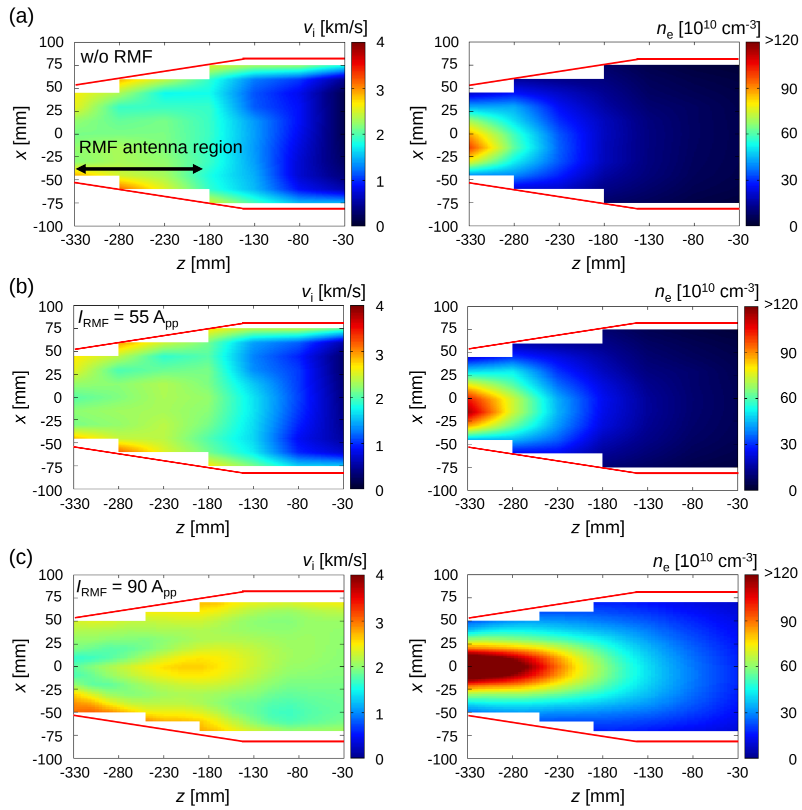

Figure 6. Spatial profiles of v_i and n_e for the case of P_{rf} = 1 kW, fr = 40 sccm, I_{RMF} = (a) 0 (w/o RMF), (b) 55, and (c) 90 A_{pp}, f_{RMF} = 0.7 MHz, and ϕ = 90°.

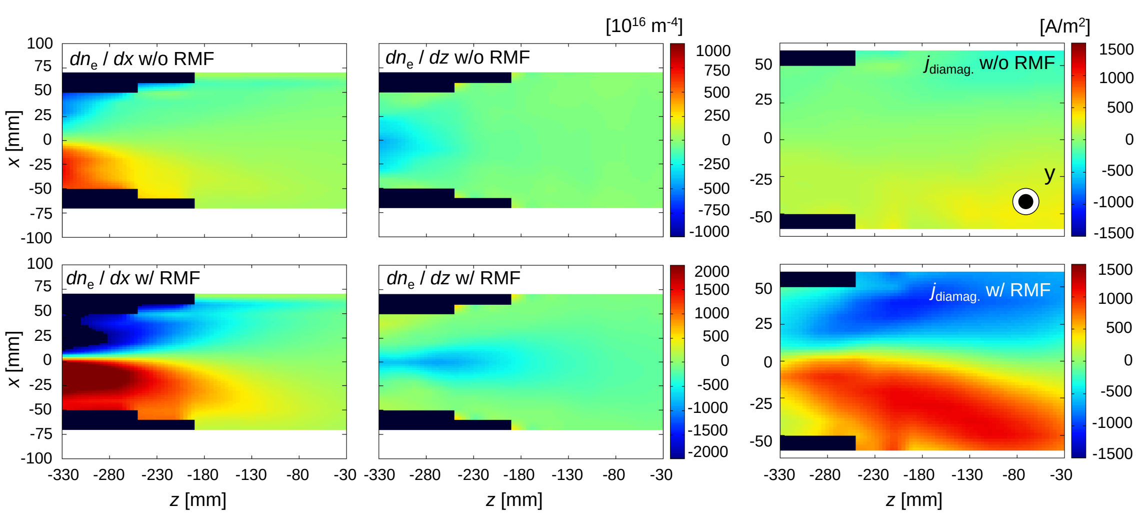

Figure 7. Spatial profiles of n_e gradient in two directions and $j_{diamag.}$ for the case of P_{rf} = 1 kW, fr = 40 sccm, I_{RMF} = 0 (upper) and 90 A_{pp} (lower), f_{RMF} = 0.7 MHz, and ϕ = 90°.

A-2. 2D spatial profiles of time-varying components of the RMF in three axes

To estimate the RMF original electromagnetic force and its B-field penetration condition into the plasma, spatial profiles of time-varying components of the RMF in three-axes were measured by the use of a B-dot probe. This measurement was conducted 37 ms after the start of the rf discharge (after 2 ms after the start of the RMF application). In terms of *x*-axis component, the B-field strength was slightly higher than that w/o RMF in the center region, indicating the RMF can penetrate into the plasma core perfectly.

In addition to such clear n_e increment in the antenna region, present RMF operational condition can be considered to yield a wave excitation mechanism, i.e., helicon wave excitation with $m = 1$.[20] In the presence of the wave excitation, theoretically, *x*- and *y*-axis components of oscillating B-fields have symmetric profiles with respect to the center axis, having a profile like the Bessel function of the 1st kind of order 0th.[20] Moreover, radial profile of the *z*-axis one has point symmetry like the function of the 1st kind of order 1th. Hereby, we can investigate qualitatively whether present plasma generation is helicon wave excitation-like or not. Based on the experimental results, the central peak of the B-fields in *x*- and *y*-directions was slightly higher than those w/o RMF application. In terms of the *z*-axis component of the RMF, the profiles look like the Bessel function of the 1st kind of order 1st.

Second harmonic components ($2f_{RMF}$) of measured B-field signals can be separated from the original f_{RMF} component through FFT (Fast Fourier Transform) analysis.[16] According to the RMF current drive method, the Hall term appears and the dc and ac second harmonic components mainly contributes to the azimuthal current drive. The second harmonic components of the azimuthal current density can be derived from radial and axial gradient of B-fields in *x* and *z* directions. In our previous experiment, the azimuthal current drive was confirmed for the I_{RMF} of 40 A_{pp} case. For optimization of the RMF electromagnetic acceleration, RMF operational conditions should be investigated in detail.

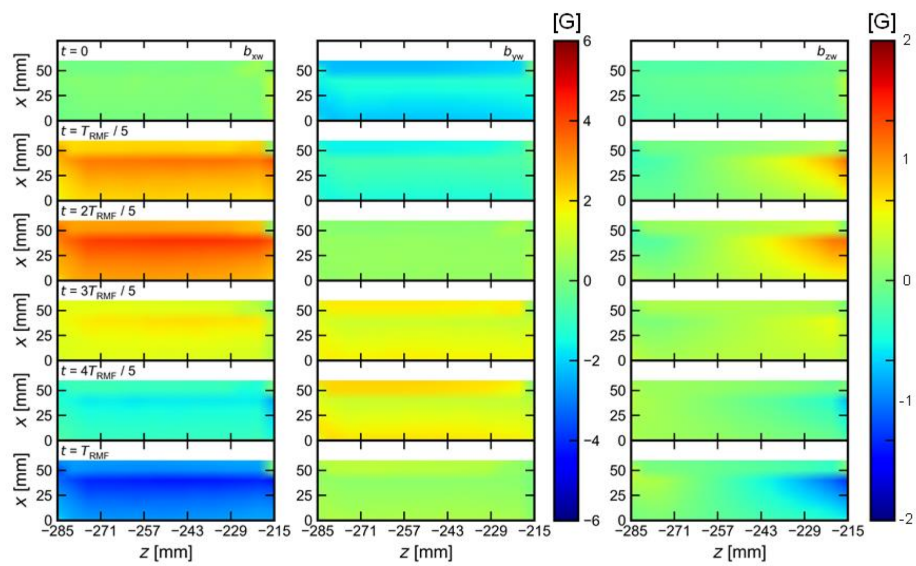

Figure 8. Spatial profiles of RMF time-varying components in three axes for the case of P_{rf} = 1 kW, *fr* = 40 sccm, I_{RMF} = 90 A_{pp}, f_{RMF} = 0.7 MHz, and ϕ = 90°.

B. Experimental results of *m* = 0 half-cycle plasma acceleration

B-1. Spatial profiles of v_i and n_e

Spatial profiles of v_i and n_e are described in this section to estimate the acceleration effect by the use of the $m = 0$ method and an rf plasma generation, as well. Here we investigated f_{m0} = 1.5 kHz case using I_{m0} = 100 A_{pp}. Time evolutions of spatial profiles of n_e, v_i, B-field shape and its field lines are described in Fig. 9. As described in Sec. II, the $m = 0$ scheme has both acceleration and deceleration phases, and for instance, $t = T_{m0} / 8$ and T_{m0} correspond to the acceleration phases and $t = T_{m0} / 2$ represents deceleration one. In the acceleration phase, the both increasing rates of n_e and v_i were the highest, compared to those in the deceleration phase. According to the theoretical manner of the $m = 0$ method, the ideal azimuthal current induction is expected to be conducted with the phase difference of 90° with respect to I_{m0} if an inductance of the plasma is much smaller than the resistance so that the former can be neglected. The spatial increase in v_i seemed to correspond to the I_{m0} peak period. In the acceleration phase, v_i peak can be seen in the radially outer region and downstream of the m = 0 antenna. This spatial characteristic can be related to the m = 0 electromagnetic acceleration effect. To estimate the m = 0 plasma acceleration effect in detail, v_i profiles in the downstream region of the m = 0 coil are also required. However, neutral pressure effect is dominant in the present experimental scheme, leading to loss of the plasma due to the collision between the accelerated plasma and the neutral particles. In addition, azimuthal current induction should be investigated to clarify the electromagnetic plasma acceleration; for example, spatiotemporal oscillating B-field measurement described in previous section and Rogowski coil method, etc.

The n_e profiles were changed by the use of m = 0 method. The n_e was increased spatially, especially, in the acceleration phase, and one of the reasons is that an ohmic heating effect would be enhanced after the current induction. Hereby, the plasma acceleration effect can be enhanced owing to the thermal thrust effect, leading to the v_i increment in the m = 0 antenna region, i.e., diamagnetic and axial pressure gradient effects, which are proportional to radial and axial density gradients, respectively, as described in the previous section.

The B-field shape and strength, which is a sum of PM field and the one by the m = 0 coil current, can be changed by increasing the I_{m0}, and in the deceleration phase, the total B-field strength can be decreased and become zero in some cases in the upstream region of the m = 0 antenna. For example, the total B-field strength was weakened at t = 3T_{m0} / 4 as shown in Fig. 9. In increasing I_{m0} value, a cusp-like field configuration can be created in the vicinity of the m = 0 antenna at this period. This can cause a forward electromagnetic force derived from the m = 0 scheme in spite of the deceleration phase. This is because the direction of the expected azimuthal current induction can be opposed to that in the acceleration phase and the radial B-field component of the external B-field can be also conversed, leading to the forward force to the evacuation direction of the thruster. Based on this acceleration mechanism, it was evident that the v_i profile was also increased in the deceleration phase at t = T_{m0} / 2, as shown in Fig. 9. As an additional acceleration mechanism, FARAD (Faraday Accelerator with Rf-Assisted Discharge)[21] scheme might be included, leading to the full-wave plasma acceleration scheme. As a future proposal, we have a plan to conduct direct thrust measurement to clarify the half-cycle (full-wave) plasma acceleration by the use of a thrust balance, launched on a thruster module with an rf plasma generation source. The increasing rates of both n_e and v_i were higher than those for I_{m0} of 100 A_{pp} case. Axial density gradient in the central plasma might be able to contribute to the larger v_i profiles in the axial center region. Ion flow along the external B-field line is expected to be clarified to optimize the plasma acceleration effect.

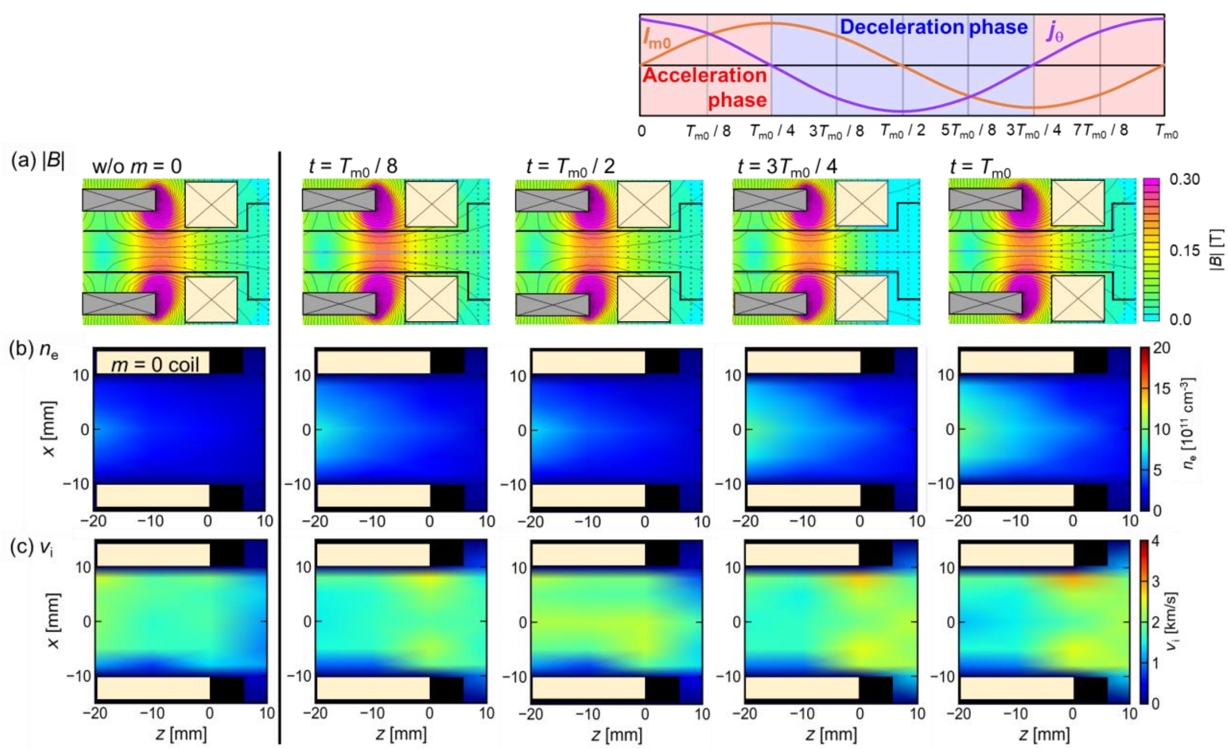

Figure 9. Time evolution of spatial profiles of (a) v_i, (b) n_e, and (c) B-field for the case of P_{rf} = 1 kW, fr = 15 sccm, I_{RMF} = 100 A_{pp}, and f_{m0} = 1.5 kHz.

Figure 10 shows dependences of normalized average n_e and v_i values on I_{m0} at (x, z) = (0, 10) and (5, 10 mm). Here, amplitudes of n_e and v_i w/ $m = 0$ application are normalized by those w/o $m = 0$ application, respectively. Both values were increased with increasing I_{m0} until I_{m0} reaches to 200 A_{pp}, but the profiles seem to be saturated for more than I_{m0} of 200 A_{pp} case. In terms of a comparison of the radial position, the v_i value was higher at $x = 5$ mm, showing the presence of the $m = 0$ electromagnetic acceleration effect.

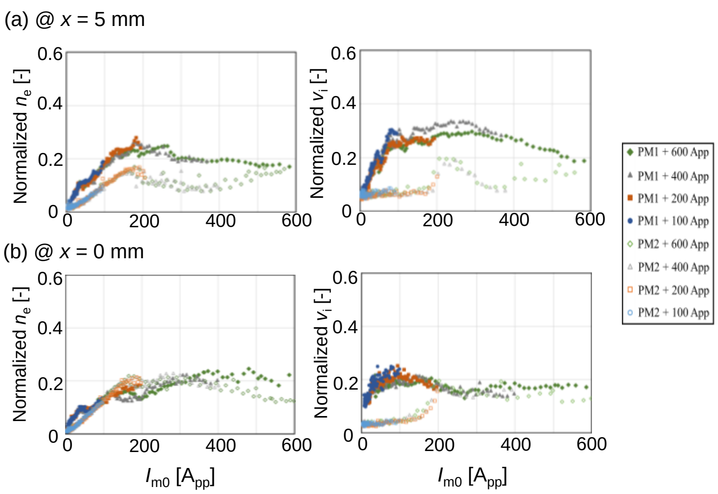

Figure 1. Dependences of n_e and v_i on I_{m0} at (r, z) = (a) (0, 10) and (b) (5 mm, 10 mm) for the case of P_{rf} = 1 kW, *fr* = 15 sccm, and f_{m0} = 1.5 kHz.

V.Conclusion

To realize next generation space missions, we are proposing two additional plasma acceleration concepts, i.e., RMF and $m = 0$ methods, in which a direct interaction of electrodes and plasma does not appear, to fulfill a completely electrodeless rf/helicon plasma thruster scheme. Here, spatial profiles of n_e, v_i, and time-varying B-field were measured to investigate the acceleration effects in these two schemes. In the RMF scheme, spatial increases of both n_e and v_i were obtained, and the increasing rates depended on the I_{RMF} value. Spatial n_e gradient becomes evident with increasing I_{RMF}, leading to high diamagnetic current density in the vicinity of the RMF antennas. In addition, the RMF time-varying components in three directions were measured by the use of a three-axis B-dot probe. Original f_{RMF} components of the RMF have the same distributions as those w/o the RMF application, that indicates the penetration condition of the RMF was enough to drive the azimuthal current. From spatiotemporal profiles of the second harmonic components of the RMF, the azimuthal current density component oscillating with $2f_{RMF}$ = 1.4 MHz can be estimated, to derive a dc component, which is the same as the $2f_{RMF}$ component theoretically, leading to the axial thrust.

The I_{RMF} value is expected to be increased, considering the RMF penetration conditions introduced by Milroy.[10] Based on present results, there can be a threshold condition that the azimuthal current drive by the use of the RMF method can be more dominant than diamagnetic current generation caused by such a high n_e gradient by the RMF application. As a future work, the detailed plasma generation mechanism by the use of the RMF method is required to optimize the RMF current drive effect and the electromagnetic force as well.

In terms of the $m = 0$ scheme, spatial n_e and v_i profiles were measured by using a Mach probe, and a relation between the external B-field and these plasma parameters was investigated. With increasing I_{m0} value proportional to the $m = 0$ B-field strength, the both parameters were increased. In addition, the oscillating components of n_e and v_i were higher in the radially outer region than those in the center region of the plasma, as shown in Fig. 9. This result shows the electromagnetic force can exist, since the azimuthal current induction is theoretically evident near the $m = 0$ coil. Quantitative evaluation of the $m = 0$ current induction is required to separate the total plasma acceleration to the original $m = 0$ and diamagnetic effect.

Acknowledgments

We appreciate prior research of the RMF acceleration method by Messrs. H. Ishii, S. Otsuka, and K. Takizawa from our group, and useful discussions made by the HEAT project members. This study has been partially supported by JSPS KAKENHI Grant Nos. JP21226019, JP17H02995, JP16K17843, and JP18J12036.

References

[1]Gold, H., "Description and Operation of Spacecraft in SERT 1 Ion Thruster Flight Test," NASA TMX-1077, 1965.

[2]Saccoccia, G., Estublier, D., and Racca, A., "SMART-1: A Technology Demonstration Mission for Science Using Electric Propulsion," *34th AIAA/ASME/SAE/ASEE Joint Propulsion Conference and Exhibit*, Cleveland, OH, July 1998, AIAA-98-3330.

[3]Chang Díaz, F. R., "The VASIMR," Scientific American, Vol. 283, No. 5, 2000, pp. 90–97.

[4]Longmier, B. W., Squire, J. P., Olsen, C. S., Cassady, L. D., Ballenger, M. G., Carter, M. D., Ilin, A. V., Glover, T. W., McCaskill, G. E., Chang Díaz, F. R., and Bering III, E. A., "Improvement Efficiency and Throttling Range of the VX-200 Magnetoplasma Thruster," *Journal of Propulsion and Power*, Vol. 30, No. 1, 2014, pp.123–132.

[5]Boswell, R. W., "Plasma production using a standing helicon wave," *Physics Letters*, Vol. 33A, No. 7, 1970, pp. 457–458.

[6]Shinohara, S., Hada, T., Motomura, T., Tanaka, K., Tanikawa, T., Toki, K., Tanaka, Y., and Shamrai, K. P., "Development of high-density helicon plasma sources and their application," *Physics of Plasmas*, Vol. 16, No. 5, 2009, pp. 057104-1–10.

[7]Shinohara, S., Nishida, H., Tanikawa, T., Hada. T., Funaki, I., Shamrai, K. P. "Development of Electrodeless Plasma Thrusters with High-density Helicon Plasma Sources," *IEEE Transactions on Plasma Science*, Vol. 42, No. 5, 2014, pp.1245–1254.

[8]Fruchtman, A., Takahashi, K., Charles, C., and Boswell, R. W., "A magnetic nozzle calculation of the force on a plasma," *Physics of Plasmas*, vol. 19, No. 3, 2012, pp. 033507-1–6.

[9]Takahashi, K., Charles, C., and Boswell, R. W., "Adiabatic Expansion of Electric Gas in a magnetic Nozzle," *Physical Review Letters*, Vol. 120, No. 4, 2018, pp. 045001-1–5.

[10]Milroy, R. D., "A numerical study of rotating magnetic fields as a current drive for field reversed configurations," *Physics of Plasmas*, Vol. 6, No. 7, 1999, pp. 2771−2780.

[11]Jones, I. R., "A review of rotating magnetic field current drive and the operation of the rotamak as a field-reversed configuration (Rotamak-FRC) and a spherical tokamak (Rotamak-ST)," *Physics of Plasmas*, Vol. 6, No. 5, 1999, pp. 1950–1957.

[12]Shinohara, S., Kuwahara, D., Ishii, T., Iwaya, H., Nishimura, S., Yamase, T., Arai, D., and Horita, H., "Development of High-Density Radio Frequency Plasma Sources With Very Small Diameter for Propulsion," *IEEE Transactions on Plasma Science*, Vol. 46, No. 2, 2018, pp. 252–262.

[13]Shinohara, S., Kuwahara, D., Furukawa, T., Nishimura, S., Yamase, T., Ishigami, Y., Horita, H., Igarashi, A., and Nishimoto, S., "Development of featured high-density helicon sources and their application to electrodeless plasma thruster," *Plasma Physics and Controlled Fusion*, Vol. 61, No. 1, 2019, pp. 014017-1–11.

[14]Furukawa, T., Takizawa, K., Kuwahara, D., and Shinohara, S., "Study on electromagnetic plasma propulsion using rotating magnetic field acceleration scheme," *Physics of Plasmas*, Vol. 24, No. 4, 2017, pp. 043505-1–7.

[15]Furukawa, T., Shimura, K., Kuwahara, D., and Shinohara, S., "Verification of azimuthal current generation employing a rotating magnetic field plasma acceleration method in an open magnetic field configuration," *Physics of Plasmas*, Vol. 26, No. 3, 2019, pp. 033505-1–7.

[16]Furukawa, T., Takizawa, K., Kuwahara, D., and Shinohara, S., "Electrodeless plasma acceleration system using rotating magnetic field method," *AIP Advances*, Vol.74, No. 11, 2017, pp. 115204-1–13.

[17]Kuwahara, D., Mishio, A., Nakagawa, T., and Shinohara, S., "Development of very small-diameter, inductively coupled magnetized plasma device," *Review of Scientific Instruments*, Vol. 84, No. 10, 2013, pp. 103502-1–4.

[18]Shinohara, S., Takechi, S., and Kawai, Y., "Effects of axial Magnetic Field and Faraday Shield on Characteristics of RF Produced Plasma Using Spiral Antenna," *Japanese Journal of Applied Physics*, Vol 35, Part 1, No. 8, 1996, pp. 4503–4508.

[19]Furukawa, T., Takizawa, K., Yano, K., Kuwahara, D., and Shinohara, S., "Spatial measurement in rotating magnetic field plasma acceleration method by using two-dimensional scanning instrument and thrust stand," *Review of Scientific Instruments*, Vol 89, No. 4, 2018, pp. 043505-1–8.

[20]Chen, F. F. and Boswell, R. W., "Helicons – The Past Decade," *IEEE transactions on Plasma Science*, Vol. 25, No. 6, 1997, pp. 1245–1257.

[21]Polzin, K. A., "Comprehensive Review of Planar Pulsed Inductive Plasma Thruster Research and Technology," *Journal of Propulsion and Power*, Vol. 27, No. 3, 2011, pp. 513–531.